Article

Discovery Medicine 2025; 37(198): 1221–1235
https://doi.org/10.24976/Discov.Med.202537198.108

Knockdown of *SIN3A* Derepresses *SYNPO2* Transcription and Inhibits Gastric Cancer Cell Progression

Fen Feng[1,†], Longqing Cheng[2,†], Qihua Xu[1], Jing Wu[1], Lirong Zhao[1], Wei Wang[1,*]

[1]Department of Gastrointestinal Oncology, Foshan First People's Hospital, 528000 Foshan, Guangdong, China
[2]Department of Anorectal Surgery, Foshan First People's Hospital, 528000 Foshan, Guangdong, China
*Correspondence: wangwei_wwang@163.com (Wei Wang)
[†]These authors contributed equally.
Published: 20 July 2025

Background: The development of novel targeted therapies for gastric cancer (GC) has been significantly hindered by our limited understanding of the molecular mechanisms underlying its progression. As SIN3 transcription regulator family member A (*SIN3A*) and synaptopodin-2 (*SYNPO2*) may influence GC progression, this study aimed to investigate the impact of *SIN3A*-mediated regulation of *SYNPO2* on GC progression.

Methods: The expression levels of *SYNPO2* and its binding interaction with *SIN3A* in GC were analyzed using bioinformatics tools. The binding sites between *SIN3A* and *SYNPO2* were validated through a dual-luciferase reporter assay. Furthermore, the biological function of *SIN3A* in regulating *SYNPO2* was investigated in GC cells using gene silencing and overexpression approaches. Cell proliferation, colony formation, apoptosis, migration, and invasion were assessed using cell counting, colony formation assay, flow cytometry, wound healing, Transwell, and molecular analyses.

Results: GC cells presented significantly reduced *SYNPO2* expression ($p < 0.01$). *SYNPO2* overexpression inhibited GC cell viability, colony formation, migration, and invasion, while promoting apoptosis ($p < 0.01$). *SYNPO2* was found to bind to *SIN3A* and mediate its transcriptional repression. *SIN3A* overexpression enhanced GC cell viability, colony formation, migration, and invasion, inhibited apoptosis, upregulated B-cell lymphoma 2 (Bcl-2), and downregulated Bcl-2-associated X protein (Bax) and cleaved caspase-3 expression, whereas *SIN3A* knockdown produced the opposite effects ($p < 0.05$). The effects of *SIN3A* knockdown were reversed by *SYNPO2* silencing in GC cells ($p < 0.05$).

Conclusion: *SIN3A* knockdown-mediated upregulation of *SYNPO2* suppresses GC malignancy processes, offering insights into a novel strategy for developing targeted therapies for gastric cancer.

Keywords: gastric cancer; SIN3 transcription regulator family member A; synaptopodin-2; cancer progression; apoptosis

Introduction

Although the incidence of gastric cancer (GC) has declined markedly over the past few decades [1], an annual rate of more than 1 million new cases remains a concerning figure [2]. GC is currently ranked as the third leading cause of cancer-related mortality worldwide [3], posing a significant public health burden. Gastric carcinogenesis is a multistage and multifactorial process [4]. However, this progression is often asymptomatic, leading to delayed diagnosis of GC, as most patients are pathologically diagnosed at advanced stages, which adversely affects prognosis [5]. While early-stage tumors can be surgically resected, advanced-stage GC often necessitates targeted therapeutic approaches [6]. Given that genetic susceptibility plays a crucial role in gastric carcinogenesis [7], recent efforts in therapeutic development have focused on identifying novel gene targets for GC treatment.

Synaptopodin-2 (*SYNPO2*, also known as myopodin), a member of the synaptopodin family, includes actin-binding and -modulating proteins [8]. *SYNPO2* promotes actin nucleation, polymerization, and bundling [9,10], and interacts with focal adhesions and associated proteins [11]. Through binding with zyxin and integrin-linked kinase, both key intracellular components of focal adhesion contact, *SYNPO2* suppresses cancer cell migratory responses [12,13]. A previous study has established SYNPO2 as a suppressor of malignant tumors [14]. SYNPO2 deficiency has been associated with an unfavorable prognosis in glioma [15], nasopharyngeal carcinoma (NPC) [16], hepatocellular carcinoma (HCC) [17], and colorectal cancer (CRC) [14]. Notably, overexpression of *SYNPO2* represses the proliferation and migration of glioma cells [15] and inhibits hypoxia-induced proliferation, migration, and invasion in CRC cells [14], while its downregulation enhances HCC cell migration and invasion [17]. Nevertheless, the

role of SYNPO2 in GC and its expression profile remain largely unexplored.

Transcription factor binding to specific DNA sequences is a key step in gene expression regulation [18]. SIN3 transcription regulator family member A (*SIN3A*) is a multifunctional transcription factor involved in inducing stem cell pluripotency, regulating cell proliferation, developmental processes, and neoplastic growth and progression [19–23]. *SIN3A* contains four paired amphipathic helix (PAH) domains, which interact with sequence-specific transcriptional regulators, and a histone deacetylase (HDAC) interaction domain (HID), which facilitates transcriptional repression by recruiting histone deacetylase 1 (HDAC1) and histone deacetylase 2 (HDAC2) [24]. According to the cancer genome atlas program (TCGA) database, *SIN3A* is highly expressed in GC. Data from the GRNdb database suggest that SIN3A regulates *SYNPO2* transcription in stomach adenocarcinoma (STAD). Therefore, we hypothesize that high *SIN3A* expression represses *SYNPO2* transcription and contributes to GC progression.

To investigate the role of *SIN3A*-mediated *SYNPO2* regulation in GC progression, we conducted gain- and loss-of-function assays by manipulating *SIN3A* and *SYNPO2* expressions in GC cells.

Materials and Methods

Bioinformatics Analysis

SYNPO2 expression pattern data for STAD tumors were obtained from the UALCAN website (https://ualcan.path.uab.edu). On the site, "TCGA" was chosen as the database, "SYNPO2" was entered as input, "stomach adenocarcinoma" was selected, the "Explore" button was clicked, followed by selection of the "Expression" tab to generate the results.

The GRNdb database (https://www.grndb.com) was utilized to predict *SIN3A* binding sites on the *SYNPO2* sequence. On the platform, "Target gene" was selected, "SYNPO2" was entered in the input panel, "Quick Search" was clicked, and "SIN3A" was entered in the search panel to retrieve the results.

Cell Culture

The human GC cell lines KATO III (HTB-103) and SNU-5 (CRL-5973) were purchased from the American Type Culture Collection (ATCC; Manassas, VA, USA). The GC cell lines MKN45 (CL-0292) and HGC27 (CL-0107), along with the normal human gastric epithelial cell line GES-1, were obtained from Sunncell (SNL-304, Wuhan, China). All cells were cultured in RPMI-1640 medium (30-2001, ATCC; Manassas, VA, USA) supplemented with 10% fetal bovine serum (FBS; 12106C, Sigma-Aldrich, St. Louis, MO, USA) and 1% penicillin-streptomycin (15140148, Thermo Fisher Scientific, Waltham, MA, USA) and incubated at 95% humidity, 5% CO_2, and 37 °C. All cell lines were authenticated using short tandem repeat (STR) profiling, and mycoplasma tests were confirmed negative.

Cell Transfection

Overexpression plasmids for *SYNPO2* (oe-*SYNPO2*) and *SIN3A* (**Supplementary File 1**), as well as short hairpin RNAs targeting *SYNPO2* and *SIN3A* (sh*SYNPO2*: 5′-GCCUCCAGAGGAUUGGAAUTT-3′ and sh*SIN3A*: 5′-CAACTGCTGAGAAGGTTGATTCTGT-3′), were procured from OriGene (RC226330, RC213240, TR307463, and TR301698, respectively; Rockville, MD, USA). pCMV6-Entry vectors (negative control, NC) and pRS vectors (PS100001 and TR20003; OriGene, Rockville, MD, USA) were utilized as controls for the overexpression plasmids and shRNAs, respectively.

HGC27 and MKN45 cells (1×10^4/well) were seeded in 96-well plates and allowed to reach approximately 90% confluence before transfection. Cells were transfected with *SYNPO2* overexpression plasmids or NC, or co-transfected with NC+shNC, shNC+*SIN3A* overexpression plasmids, NC+sh*SIN3A,* or sh*SIN3A*+sh*SYNPO2* using Lipofectamine 3000 transfection reagent (L3000015, Thermo Fisher Scientific, Waltham, MA, USA). After 48 hours, quantitative reverse transcription polymerase chain reaction (qRT-PCR) was performed to assess transfection efficiency.

Quantitative Reverse Transcription Polymerase Chain Reaction (qRT-PCR)

Total RNA was extracted from non-transfected and transfected HGC27 and MKN45 cells using Trizol reagent (15596026, Thermo Fisher Scientific, Waltham, MA, USA). cDNA synthesis was performed using the Hiscript QRT SuperMix (R122-01, Vazyme, Nanjing, China). The qRT-PCR reactions were performed on a thermal cycler (ABI 7500, Thermo Fisher Scientific, Waltham, MA, USA). Thermocycling conditions were as follows: predenaturation at 95 °C, followed by 40–45 cycles of 95 °C for 10 s and 60 °C for 30 s. Glyceraldehyde-3-phosphate dehydrogenase (*GAPDH*) was used as the internal reference gene, and relative gene expression levels were calculated using the $2^{-\Delta\Delta Ct}$ method [25]. The primers used (5–3′) were as follows: *SYNPO2*, forward (F): AGAAGCAGCCCTTACAAGTTG, and reverse (R): AGCCTCACTTATTCCACTGGAT; *SIN3A*, F: ACCATGCAGTCAGCTACGG, and R: CACCGCTGTTGGGTGATGA; *GAPDH*, F: GGAGCGAGATCCCTCCAAAAT, and R: GGCTGTTGTCATACTTCTCATGG.

Dual-Luciferase Reporter Assay

Site-directed mutagenesis of the wild-type (WT) *SYNPO2* sequence was carried out using the GeneTailor Site-Directed Mutagenesis System (12397-014, Invitrogen, Carlsbad, CA, USA). The WT (5′-

CCGGCGGCGCCGGCGGGGGG-3′) and mutant (MUT; 5′-CCGGTGGCGCCGGCGCGGGG-3′) sequences were individually cloned into pGL3 luciferase vectors (E1761, Promega, Madison, WI, USA). These constructs were co-transfected into HGC27 and MKN45 cells together with *SIN3A* overexpression plasmids or NC and the pRL-TK plasmid (E2241, Promega, Madison, WI, USA), which served as an internal control. After 48 hours, cells were lysed and analyzed using the Dual-Luciferase Reporter Assay System (E1980, Promega, Madison, WI, USA) and a fluorescence microplate reader (Infinite M1000, Tecan, Morrisville, NC, USA). Relative luciferase activity was calculated as the ratio of firefly luciferase to Renilla luciferase activity, and normalized to the NC group.

Cell Counting Kit-8 (CCK-8) Assay

Transfected and non-transfected HGC27 and MKN45 cells were seeded into 96-well plates (2×10^3/well) and incubated for 24, 48, or 72 hours at 37 °C. Subsequently, 10 µL of CCK-8 reagent (CA1210, Solarbio, Beijing, China) was added to each well and incubated for 2 hours. The optical density (OD) was measured at 450 nm using a microplate reader (EMax Plus, Molecular Devices, Sunnyvale, CA, USA). Cell viability was calculated using the following formula:

Cell viability (OD value) = [(OD_treatment group – OD_blank group) / (OD_control group – OD_blank group)].

Colony Formation Assay

HGC27 and MKN45 cells, with or without transfection, were seeded into 6-well plates (1×10^3 cells/well) and cultured for 3 weeks. Once visible colonies had formed, the cell layers were washed with phosphate-buffered saline (PBS; #9808, Cell Signaling Technology, Danvers, MA, USA), fixed with 4% paraformaldehyde (158127, Sigma-Aldrich, St. Louis, MO, USA) for 15 minutes, and stained with 0.1% crystal violet (X11099, Xiaoyou Biotechnology, Hangzhou, China) for 25 minutes. Colony images were captured using a digital camera (D850, NIKON, Tokyo, Japan). Relative colony numbers were calculated using the formula:

Relative colony number = (Colonies in experimental group) / (Colonies in blank group).

All data were normalized to the blank group.

Flow Cytometry

Cell apoptosis detection was performed using the Annexin V-FITC Early Apoptosis Detection Kit (#6592, Cell Signaling Technology, Danvers, MA, USA). Briefly, transfected and non-transfected HGC27 and MKN45 cells were centrifuged at 2000 ×g for 10 minutes, rinsed with pre-cooled PBS, and resuspended in Annexin-V binding buffer to a final density of 1×10^6 cells/mL. A 96 µL aliquot of the cell suspension was incubated with 1 µL Annexin V-FITC and 12.5 µL propidium iodide for 10 minutes on ice in the dark. The cell mixture was then diluted with Annexin-V binding buffer to a total volume of 250 µL and analyzed using a flow cytometer (Cytoflex, Beckman Coulter, Brea, CA, USA). The apoptosis rate was determined using the following formula:

Apoptosis rate = early apoptosis + late apoptosis.

Wound Healing Assay

Transfected and non-transfected HGC27 and MKN45 cells were seeded into 24-well plates (1.25×10^5 cells/well) with serum-free media and starved for 24 hours. Upon reaching 100% confluence, the culture media were replaced with medium supplemented with 10% FBS. A streak was introduced across the monolayer using a sterile pipette tip, followed by PBS washing to remove detached cells. The streak width and time of wound formation were recorded as 0 hours. After 48 hours, wound closure was photographed using an inverted microscope (100× magnification; DMi8, Leica, Wetzlar, Germany). The relative migration rate was determined as follows:

Relative migration rate (%) = [(0 hours scratch width – 48 hours scratch width) / 0 hours scratch width] × 100%.

All data were normalized to the blank group.

Transwell Assay

The Transwell assay was conducted based on a previously described method [26], with minor modifications. Briefly, transfected and non-transfected HGC27 and MKN45 cells were resuspended in 200 µL serum-free medium to a final density of 1×10^5 cells/mL. The suspensions were added to the upper chambers and filled with 8-µm pore size Transwell inserts (3428, Corning Inc., Corning, NY, USA), pre-coated with 50 µL Matrigel (1 mg/mL; 356234, Corning Inc., Corning, NY, USA). The lower chambers were filled with culture medium containing 20% FBS as a chemoattractant. After incubation at 37 °C for 48 hours, non-invading cells on the upper surface were removed. The invaded cells on the lower membrane surface were fixed in 4% paraformaldehyde for 10 minutes and stained with 0.1% crystal violet for 15 minutes. Cells were counted using an inverted microscope (ECLIPSE Ts2R, Nikon, Shanghai, China) at 100× magnification.

Relative invasion rate = (Number of invading cells in experimental group) / (Number of invading cells in blank group).

All results were normalized to the blank group.

Western Blotting

Total protein was extracted from transfected and non-transfected HGC27 and MKN45 cells using Radio-Immunoprecipitation Assay (RIPA) buffer (89901, Thermo Fisher Scientific, Waltham, MA, USA) supplemented with protease inhibitor reagents (87785, Thermo Fisher Scien-

tific, Waltham, MA, USA). Total protein concentration was quantified using a Bicinchoninic Acid (BCA) Protein Assay Kit (A53227, Thermo Fisher Scientific, Waltham, MA, USA). Proteins were then separated by sodium dodecyl-sulfate-polyacrylamide gel electrophoresis (SDS-PAGE) using commercially available gels (1615100, BIO-RAD, Hercules, CA, USA), and subsequently transferred onto PVDF membranes (ISEQ00010, Sigma-Aldrich, St. Louis, MO, USA). Membrane were blocked in 5% bovine serum albumin (37520, Thermo Fisher Scientific, Waltham, MA, USA) for 2 hours at room temperature (RT), followed by overnight incubation at 4 °C with primary antibodies against B-cell lymphoma 2 (Bcl-2) (#4223, 26 kDa, 1:1000), Bcl-2-associated X protein (Bax) (#5023, 20 kDa, 1:1000), and GAPDH (#5174, 37 kDa, 1:1000) (all from Cell Signaling Technology, Danvers, MA, USA), and cleaved caspase-3 (ab2302, 17 kDa, 1:500; Abcam, Cambridge, UK). After Phosphate-Buffered Saline (PBS) Tween-20 (28360, Thermo Fisher Scientific, Waltham, MA, USA) washing, membranes were incubated with horseradish peroxidase (HRP)-conjugated anti-rabbit secondary antibodies (31460, Thermo Fisher Scientific, Waltham, MA, USA) for 1 hour at RT. Immunoreactive bands were visualized using Luminol Reagent (sc-2048, Santa Cruz, Dallas, TX, USA) on an imaging system (EC3, UVP, Upland, CA, USA). Band intensity was quantified using ImageJ software (version 3.0; National Institutes of Health, Bethesda, MD, USA). Relative protein expression was calculated as follows:

Relative protein expression level = (Gray value of target protein) / (Gray value of loading control).

All data were normalized to the blank group.

Statistical Analyses

All statistical analyses were conducted using SPSS software (version 20.0; SPSS Inc., Chicago, IL, USA). The association between *SYNPO2* expression and clinicopathological parameters of GC patients was assessed using Chi-square tests. Quantitative data were presented as mean ± standard deviation (SD). Paired *t*-tests were used to compare GC tissues with adjacent normal tissues, while independent *t*-tests were applied for comparisons between different groups. One-way analysis of variance (ANOVA) followed by Tukey's post hoc test was conducted for multiple group comparisons. A p-value < 0.05 was considered statistically significant.

Results

SYNPO2 Expression was Decreased in GC Cells, and GC Cell Viability Declined Following SYNPO2 Overexpression

Analysis using data from the UALCAN database revealed that *SYNPO2* expression was significantly lower in primary STAD tissues than in normal tissues ($p < 0.01$, Fig. 1A). Using qRT-PCR, we confirmed that *SYNPO2* was downregulated in GC cell lines (MKN45 ($p < 0.001$), HGC27 ($p < 0.001$), and SNU-5 ($p < 0.01$)), relative to GES-1 cells (Fig. 1B). Subsequently, MKN45 and HGC27 cells were individually transfected with *SYNPO2* overexpression plasmids, given that *SYNPO2* expression was lower in these two lines relative to the other GC cells tested. Following plasmid transfection, *SYNPO2* expression was significantly upregulated in the two cell lines ($p < 0.001$, Fig. 1C,D). Cell viability was then detected and found to be significantly reduced at 48 hours ($p < 0.01$) and 72 hours (HGC27 cells: $p < 0.001$; MKN45: $p < 0.01$) post-transfection with the *SYNPO2* overexpression plasmid (Fig. 1E,F).

SYNPO2 Overexpression Impeded GC Cell Colony Formation, Migration, and Invasion, While Enhancing Apoptosis

MKN45 and HGC27 cells overexpressing *SYNPO2* showed a markedly reduced capacity to form colonies ($p < 0.01$, Fig. 2A,B) and a significantly increased rate of cell apoptosis ($p < 0.001$, Fig. 2C,D). Additionally, migration and invasion capacities of MKN45 and HGC27 cells transfected with the *SYNPO2* overexpression plasmid were significantly decreased ($p < 0.05$, Fig. 3A–D).

SYNPO2 was Downregulated by SIN3A in GC Cells Through Direct Binding

Binding sites within the *SYNPO2* sequence complementary to *SIN3A* were determined using the GRNdb database (Fig. 4A), followed by *in silico* analysis of the interaction between *SIN3A* and *SYNPO2*. qRT-PCR results indicated that *SIN3A* expression was significantly upregulated following transfection with *SIN3A* overexpression plasmid and downregulated after transfection with sh*SIN3A* plasmid in MKN45 and HGC27 cells ($p < 0.001$, Fig. 4B,C). Luciferase activity was significantly reduced in MKN45 and HGC27 cells co-transfected with *SIN3A* overexpression plasmids and *SYNPO2*-WT, compared to those co-transfected with NC and *SYNPO2*-WT ($p < 0.01$, $p < 0.001$, Fig. 4D,E). However, luciferase activity in MKN45 and HGC27 cells containing *SYNPO2*-MUT was not significantly attenuated after transfection with *SIN3A* overexpression plasmids (Fig. 4D,E). Furthermore, *SYNPO2* gene silencing decreased its expression in MKN45 and HGC27 cells ($p < 0.001$, Fig. 4F,G). Moreover, qRT-PCR analysis validated the regulatory effect of *SIN3A* on *SYNPO2* expression in GC cells, as *SIN3A* overexpression significantly decreased *SYNPO2* expression levels in MKN45 and HGC27 cells ($p < 0.001$, Fig. 4F,G).

SIN3A Regulated SYNPO2 Expression to Modulate GC Cell Viability

SYNPO2 expression was significantly reduced in MKN45 and HGC27 cells following transfection with the

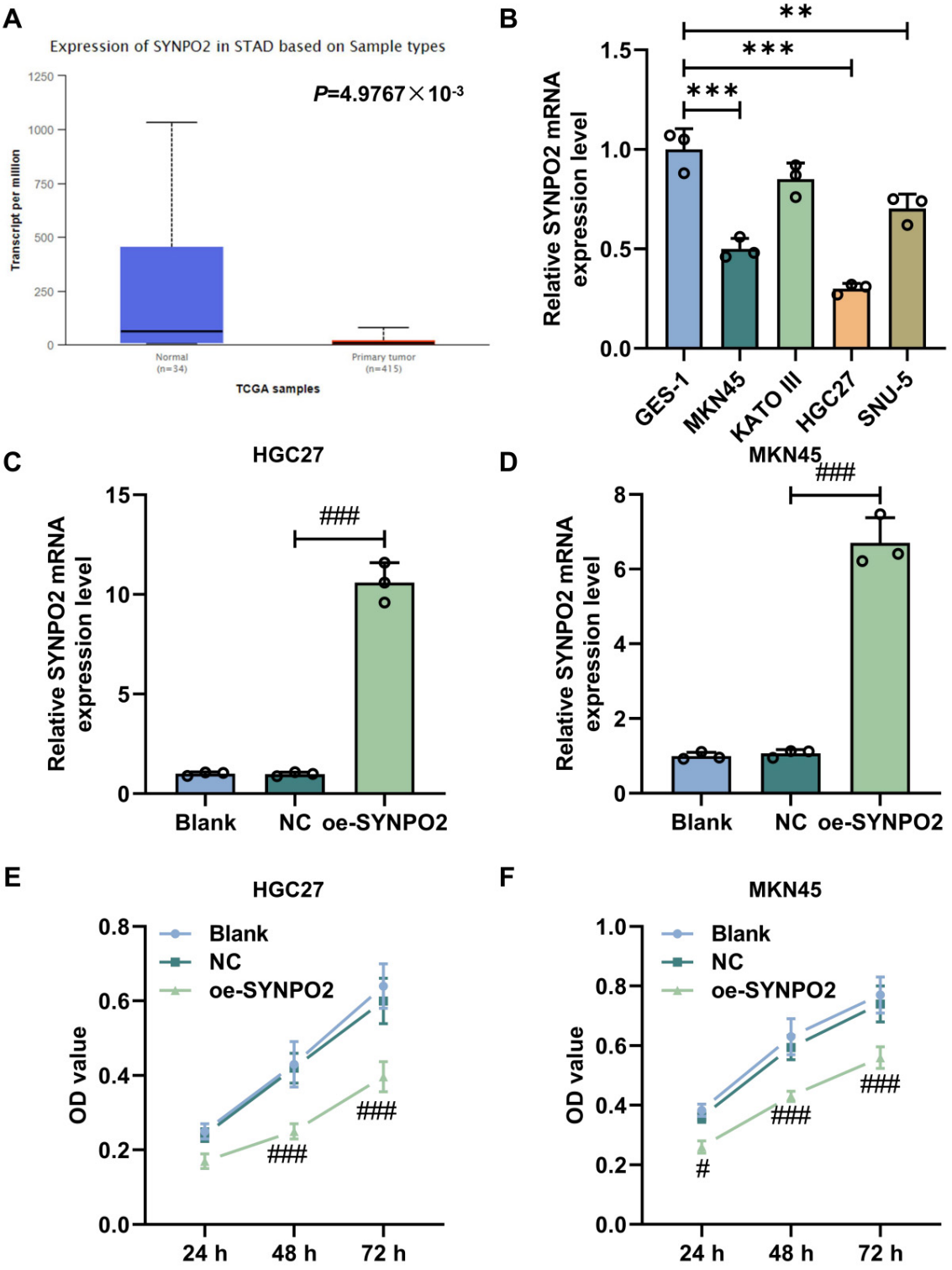

Fig. 1. Low *SYNPO2* expression in GC cells and reduced cell viability following *SYNPO2* overexpression. (A) Expression levels of *SYNPO2* in STAD tumor tissues (n = 415) and normal samples (n = 34) obtained from the UALCAN database. (B) *SYNPO2* expression in GC cells and GES-1 cells assessed by qRT-PCR (*GAPDH* as the internal control), $^{**}p < 0.01$, $^{***}p < 0.001$ vs. GES-1. (C,D) *SYNPO2* expression in HGC27 and MKN45 cells transfected with *SYNPO2* overexpression plasmids or NC determined by qRT-PCR (*GAPDH* as the internal control), $^{###}p < 0.001$ vs. NC. (E,F) Viability of HGC27 and MKN45 cells transfected with *SYNPO2* overexpression plasmids or NC, measured at 24, 48, and 72 hours using the Cell Counting Kit-8 (CCK-8) assay, $^{#}p < 0.05$, $^{###}p < 0.001$ vs. NC. n = 3. GC, gastric cancer; STAD, stomach adenocarcinoma; *SYNPO2*, synaptopodin-2; NC, negative control; qRT-PCR, quantitative reverse-transcription polymerase chain reaction; GAPDH, Glyceraldehyde-3-phosphate dehydrogenase.

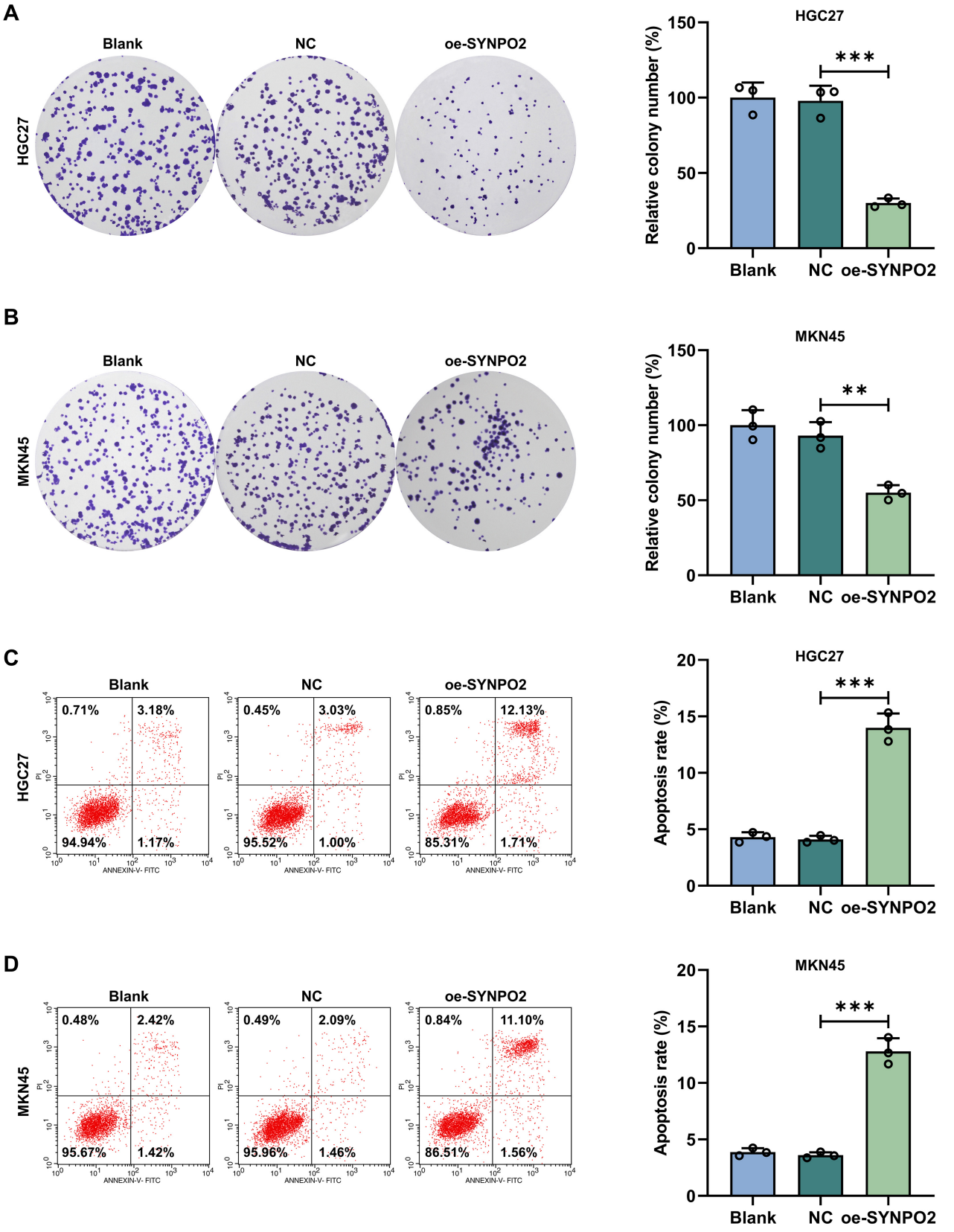

Fig. 2. *SYNPO2* overexpression inhibits GC cell colony formation and promotes apoptosis. (A,B) Colony formation assay showing reduced colony-forming ability in HGC27 (A) and MKN45 (B) cells transfected with *SYNPO2* overexpression plasmids or NC. (C,D) Flow cytometric analysis of apoptosis in HGC27 (C) and MKN45 (D) cells following transfection with *SYNPO2* overexpression plasmids or NC. $^{**}p < 0.01$, $^{***}p < 0.001$; n = 3.

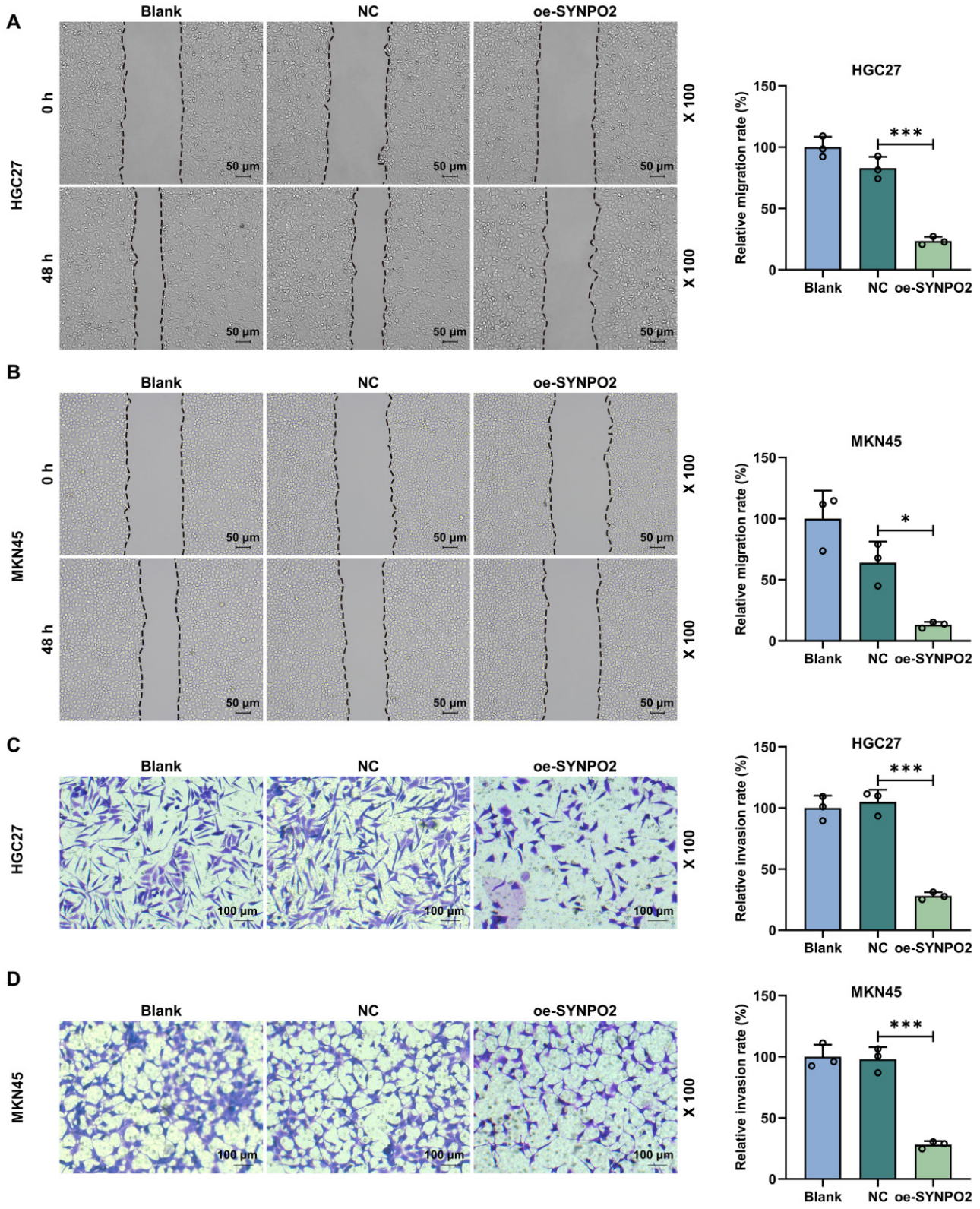

Fig. 3. *SYNPO2* overexpression suppresses migration and invasion of GC cells. (A,B) Wound healing assay showing impaired migratory ability in HGC27 (A) and MKN45 (B) cells transfected with *SYNPO2* overexpression plasmids or NC (magnification: ×100; scale bar: 50 μm). (C,D) Transwell invasion assay showing reduced invasiveness in HGC27 (C) and MKN45 (D) cells transfected with *SYNPO2* overexpression plasmids or NC (magnification: ×100; scale bar: 100 μm). *$p < 0.05$, ***$p < 0.001$; n = 3.

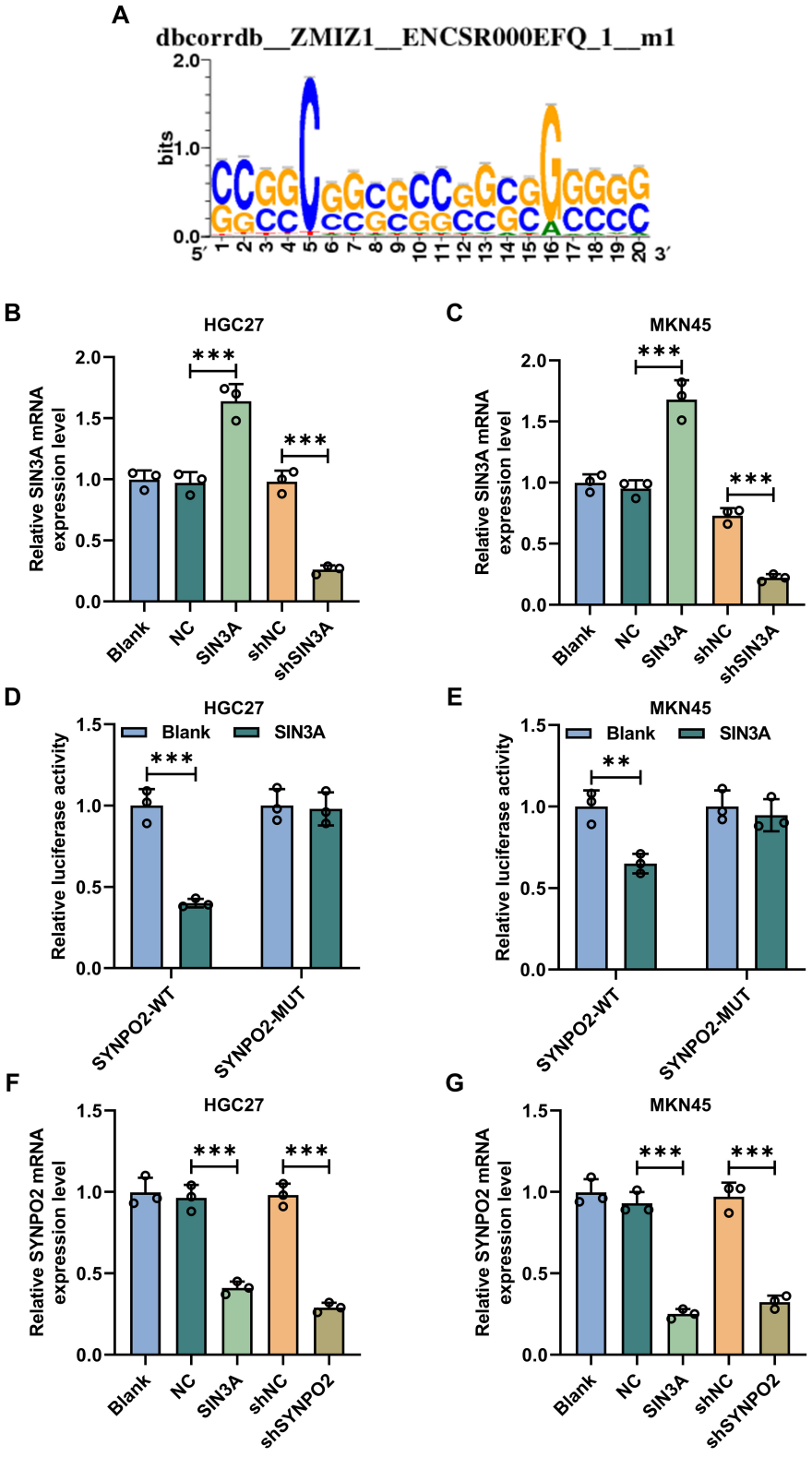

Fig. 4. Downregulation of *SYNPO2* expression by *SIN3A* following binding in GC cells. (A) Predicted *SIN3A* binding sites complementary to the *SYNPO2* sequence retrieved from the GRNdb database. (B,C) *SIN3A* expression in HGC27 and MKN45 cells transfected with *SIN3A* overexpression plasmids or NC, assessed by qRT-PCR (*GAPDH* as the internal control). (D,E) Regulatory relationship between *SYNPO2* and *SIN3A* in HGC27 and MKN45 cells analyzed via dual-luciferase reporter assay. (F,G) *SYNPO2* expression in *SIN3A* overexpression, shSYNPO2 plasmids or NC-transfected HGC27 and MKN45 cells measured by qRT-PCR (*GAPDH* as the internal control). $^{**}p < 0.01$, $^{***}p < 0.001$; n = 3. WT, wild-type; MUT, mutant.

SIN3A overexpression plasmid, but was elevated after *SIN3A* knockdown ($p < 0.001$, Fig. 5A,B). Furthermore, *SYNPO2* knockdown reversed the upregulation of *SYNPO2* induced by *SIN3A* knockdown in MKN45 and HGC27 cells ($p < 0.001$, Fig. 5A,B). *SIN3A* overexpression significantly increased the viability of MKN45 and HGC27 cells, while *SIN3A* knockdown decreased cell viability ($p < 0.05$, Fig. 5C,D). Notably, the inhibitory effect of *SIN3A* knockdown on cell viability was reversed by *SYNPO2* knockdown ($p < 0.05$, Fig. 5C,D).

SIN3A-Mediated SYNPO2 Expression Modulated GC Cell Colony Formation and Apoptosis

Colony formation of MKN45 and HGC27 cells was significantly enhanced by *SIN3A* overexpression and repressed by *SIN3A* knockdown ($p < 0.05$, Fig. 6A,B). However, *SYNPO2* knockdown reversed the inhibition of cell colony formation caused by *SIN3A* knockdown ($p < 0.001$, Fig. 6A,B). Additionally, *SIN3A* overexpression significantly suppressed apoptosis in MKN45 and HGC27 cells ($p < 0.05$, Fig. 6C,D). Conversely, *SIN3A* knockdown promoted apoptosis, an effect counteracted by *SYNPO2* knockdown ($p < 0.001$, Fig. 6C,D).

SIN3A-Mediated Regulation of SYNPO2 Expression Modulated GC Cell Migration and Invasion

MKN45 and HGC27 cells overexpressing *SIN3A* exhibited significantly aggressive migration and invasion capabilities, whereas *SIN3A* knockdown reduced these aggressive behaviors ($p < 0.05$, Fig. 7A–D). Notably, *SYNPO2* silencing reversed the inhibitory effects of *SIN3A* silencing on GC cell migration and invasion ($p < 0.01$, $p < 0.05$, Fig. 7A–D).

SIN3A-Mediated Regulation of SYNPO2 Expression Influenced Apoptosis-Related Protein Expression in GC Cells

In the present study, we observed that *SIN3A* overexpression increased Bcl-2 expression and suppressed the expression of Bax and cleaved caspase-3 in MKN45 and HGC27 cells ($p < 0.001$, Fig. 8A–D). As expected, *SIN3A* knockdown exerted an opposite effect on the levels of these apoptosis-related proteins in MKN45 and HGC27 cells ($p < 0.001$, Fig. 8A–D). Notably, the effects of *SIN3A* knockdown were reversed by *SYNPO2* knockdown ($p < 0.001$, Fig. 8A–D).

Discussion

The incidence of GC presents a progressive increase with age [27], making it a major clinical challenge in the global population ageing. Given that gastric carcinogenesis is a multifactorial and multistage process involving extensive gene expression alterations, which are key drivers of GC pathogenesis [27], identifying aberrantly expressed genes associated with malignant progression, may provide invaluable insights for the development of novel targeted therapies.

During cancer progression, the cytoskeletal components, including actin filaments, microtubule networks, and intermediate filaments, undergo dynamic remodeling, a key process that promotes the migration of cancer cells [28]. SYNPO2 is an actin-binding protein capable of inducing actin polymerization and bundling [9], contributing to the structural reorganization of the actin network and regulation of cell migration [29]. The upregulation of *SYNPO2*, considered an oncogene, has been significantly associated with poor prognosis in nasopharyngeal carcinoma patients [16]. Given that actin polymerization is essential for cell invasion [30], *SYNPO2* is hypothesized to promote cancer progression by inducing actin network remodeling. This concept has been corroborated by several studies. For instance, *SYNPO2*-mediated formation of distinct actin networks, morphologically and biochemically, has been associated with prostate cancer cell migration [31]. Moreover, *SYNPO2* has been shown to enhance the formation of nascent focal adhesions and peripheral actin bundles, thereby facilitating the migratory capacity of prostate cancer cells [11].

However, numerous studies have reported that *SYNPO2* functions as a tumor suppressor. Low *SYNPO2* expression or mutation has been shown to activate signaling pathways, including phosphoinositide 3-kinase/protein kinase B/mammalian target of rapamycin (PI3K/AKT/mTOR) and large tumor suppressor kinase 2/Yes-associated protein/transcriptional coactivator with PDZ-binding motif (LATS2/YAP/TAZ), thereby promoting cancer progression [8]. For instance, *SYNPO2* is lost in breast cancer (BC), HCC, and hypoxia-exposed CRC cells. Notably, *SYNPO2* overexpression repressed the migratory and invasive phenotypes of HCC and hypoxia-exposed CRC cells [14,17], while its downregulation promoted the migration and invasion in HCC and BC cells [17,32]. Apoptosis is a primary mechanism underlying targeted cancer therapy [33]. *SYNPO2* overexpression has been shown to promote apoptosis in CRC cells [14]. Similarly, our study revealed a tumor-suppressive role of *SYNPO2* in GC cells, as supported by its negative correlation with invasion depth, TNM stage, and lymph node metastasis. Additionally, *SYNPO2* overexpression suppressed GC cell proliferation, migration, and invasion while enhancing apoptosis.

Notably, in HCC cells, *SYNPO2* expression is inversely correlated with malignant cell features. The nuclear-to-cytoplasmic translocation of *SYNPO2*, observed in recurrent HCC patients, accelerates peripheral actin bundle assembly, thereby promoting HCC metastasis [17]. Moreover, in normal gastric mucosa, *SYNPO2* is expressed at almost undetectable levels in stromal cells. Conversely, it is mainly expressed in tumor cells, fibroblasts, and in-

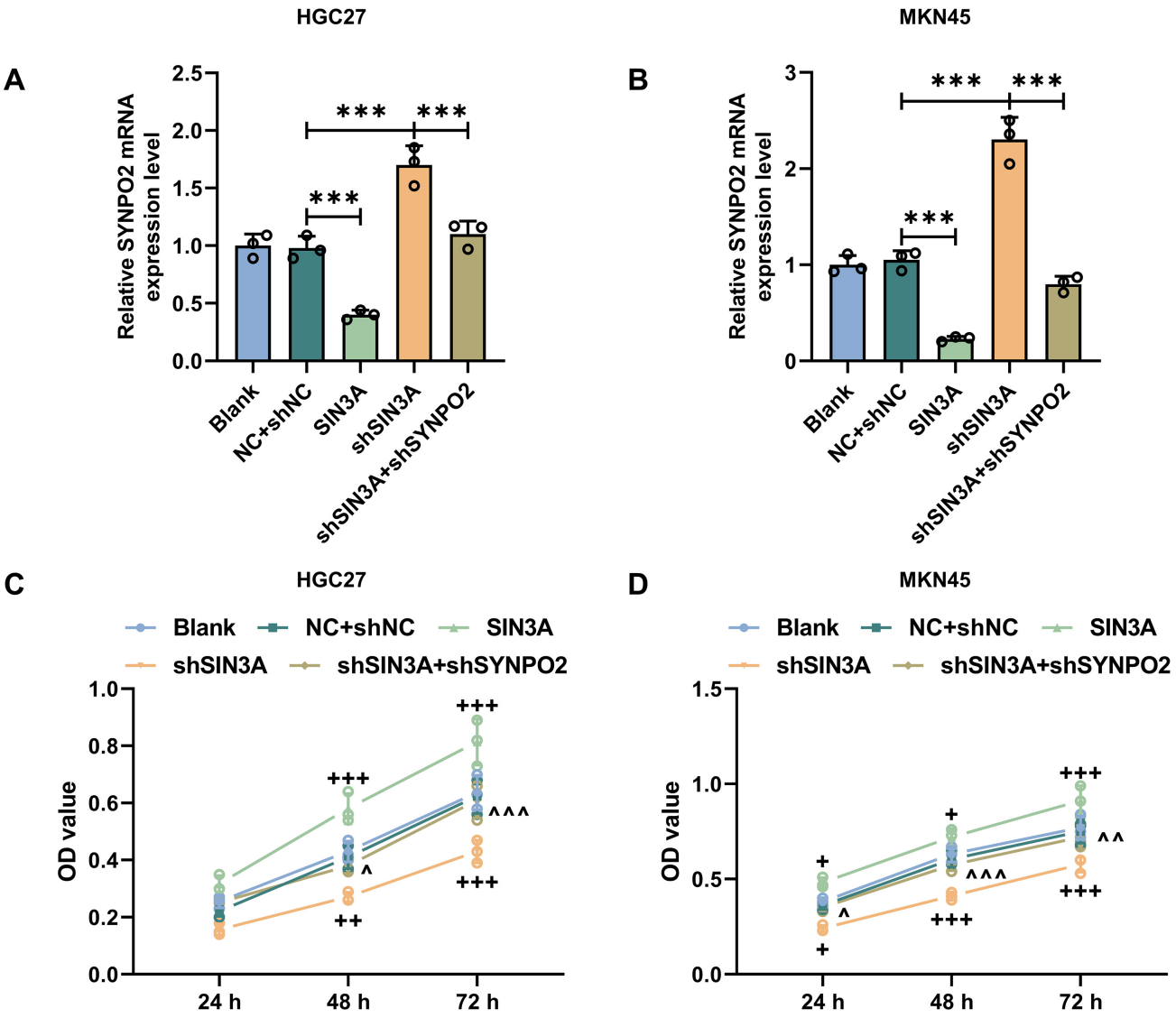

Fig. 5. SIN3A-mediated regulation of *SYNPO2* expression modulates GC cell viability. (A,B) *SYNPO2* expression in GC cells co-transfected with NC+shNC, *SIN3A* overexpression plasmid, sh*SIN3A*, or sh*SIN3A*+sh*SYNPO2* was analyzed by qRT-PCR (*GAPDH* as the internal control). (C,D) Cell viability of HGC27 and MKN45 cells co-transfected with NC+shNC, *SIN3A* overexpression plasmid, sh*SIN3A*, or sh*SIN3A*+sh*SYNPO2* at 24, 48, and 72 hours was assessed by Cell Counting Kit-8 (CCK-8) assay. ***$p < 0.001$; n = 3; $^{+}p < 0.05$, $^{++}p < 0.01$, $^{+++}p < 0.001$, vs. NC+shNC; $^{\wedge}p < 0.05$, $^{\wedge\wedge}p < 0.01$, $^{\wedge\wedge\wedge}p < 0.001$ vs. sh*SIN3A*. n = 3. sh*SIN3A*, short hairpin RNA targeting *SIN3A*; shNC, short hairpin RNA against NC.

flammatory cells (including eosinophils and lymphocytes) within GC tissue and is associated with elevated peritoneal metastasis in GC patients [34]. In this study, we observed that *SYNPO2* expression levels varied across the GC cell lines examined. This variation suggests that distinct disease outcomes among patients may be attributed to the different mechanisms mediated by *SYNPO2* within the same cancer type or among different GC cell lines. Notably, SYNPO2 protein expression was not investigated in this study. Therefore, further research should be conducted to determine whether SYNPO2 enhances peripheral actin bundling to facilitate GC metastasis. Interestingly, our study is the first to demonstrate that *SYNPO2* expression is repressed by *SIN3A* in GC cells, suggesting that *SIN3A* may exert a negative regulatory effect on *SYNPO2* expression.

Predicted using the data available in the GRNdb database, *SIN3A*, a transcription factor, regulates *SYNPO2* transcription in stomach adenocarcinoma (STAD). Activation of the pro-apoptotic Bax neutralizes the anti-apoptotic activity of Bcl-2, leading to the release of cytochrome c, which subsequently activates caspase-3 and ultimately induces apoptosis [35]. Our data indicated an anti-apoptotic role for *SIN3A* in GC cells, as evidenced by *SIN3A*-mediated inverse regulation of apoptosis, Bax and cleaved caspase-3, and the positive regulation of Bcl-2 expression. The HID domain of *SIN3A* enables the recruitment

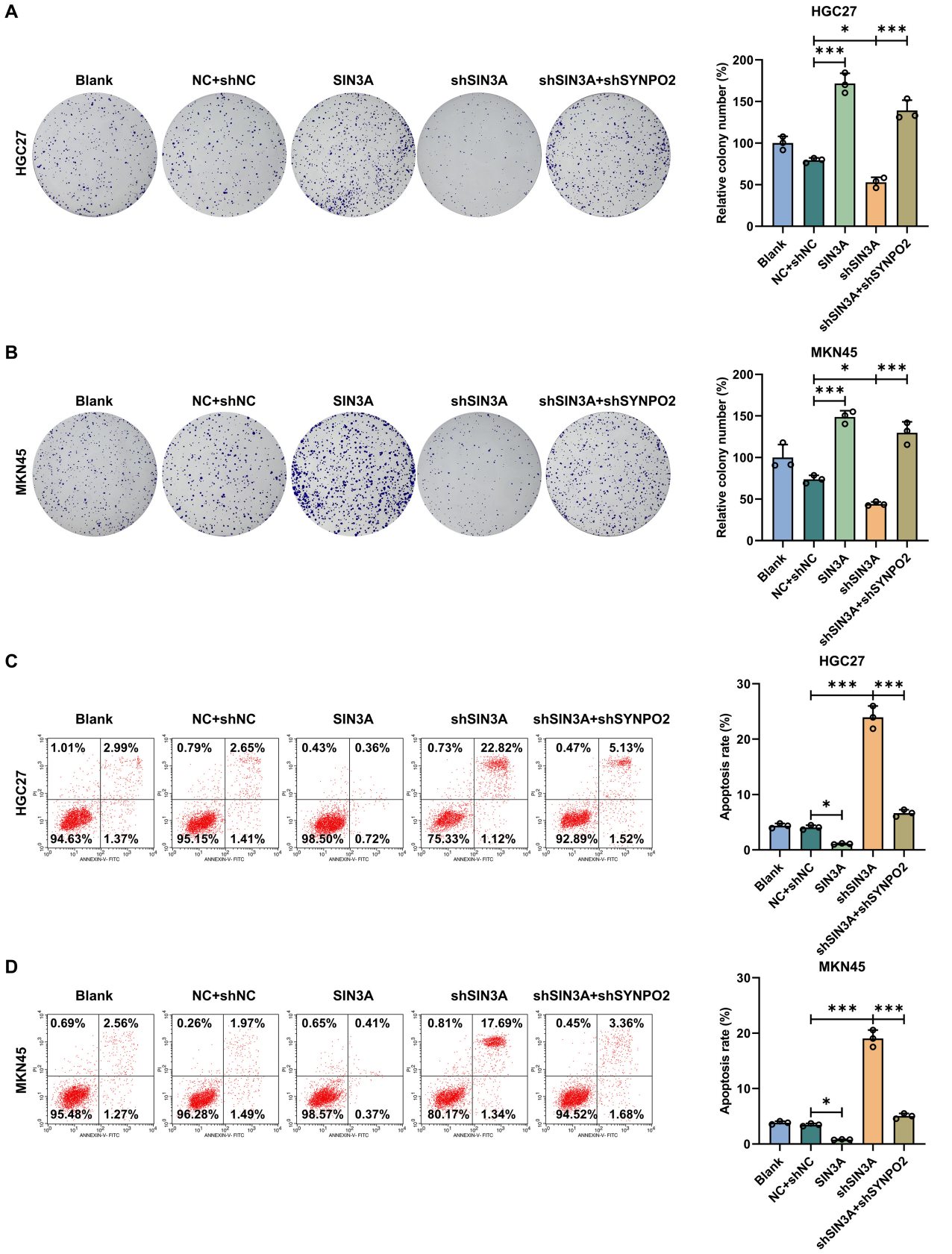

Fig. 6. *SIN3A*-mediated repression of *SYNPO2* expression promotes colony formation and inhibits apoptosis in GC cells. (A,B) Colony formation assay in GC cells co-transfected with NC+shNC, *SIN3A* overexpression plasmid, sh*SIN3A,* or sh*SIN3A*+sh*SYNPO2*. (C,D) Apoptosis of GC cells co-transfected with NC+shNC, *SIN3A* overexpression plasmid, sh*SIN3A,* or sh*SIN3A*+sh*SYNPO2* evaluated by flow cytometry. *$p < 0.05$, ***$p < 0.001$; n = 3.

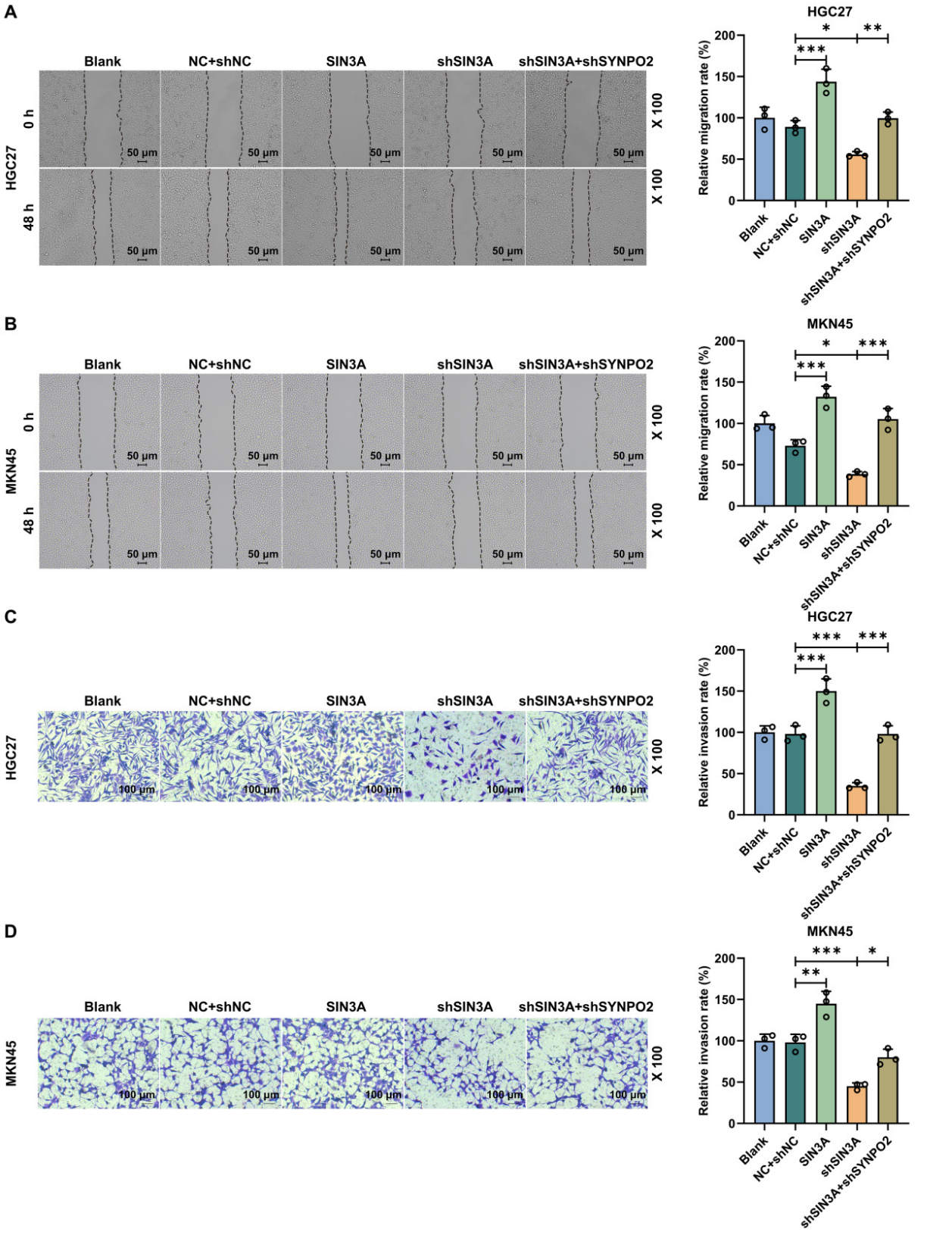

Fig. 7. *SIN3A*-mediated regulation of *SYNPO2* promotes GC cell migration and invasion. (A,B) Migration capacity of GC cells co-transfected with NC+shNC, *SIN3A* overexpression plasmids, sh*SIN3A*, or sh*SIN3A*+sh*SYNPO2* was assessed using wound healing assay (magnification: ×100; scale bar: 50 μm). (C,D) Invasive potential of GC cells co-transfected with NC+shNC, *SIN3A* overexpression plasmids, sh*SIN3A*, or sh*SIN3A*+sh*SYNPO2*, was evaluated by Transwell assay (magnification: ×100; scale bar: 100 μm). *$p < 0.05$, **$p < 0.01$, ***$p < 0.001$; n = 3.

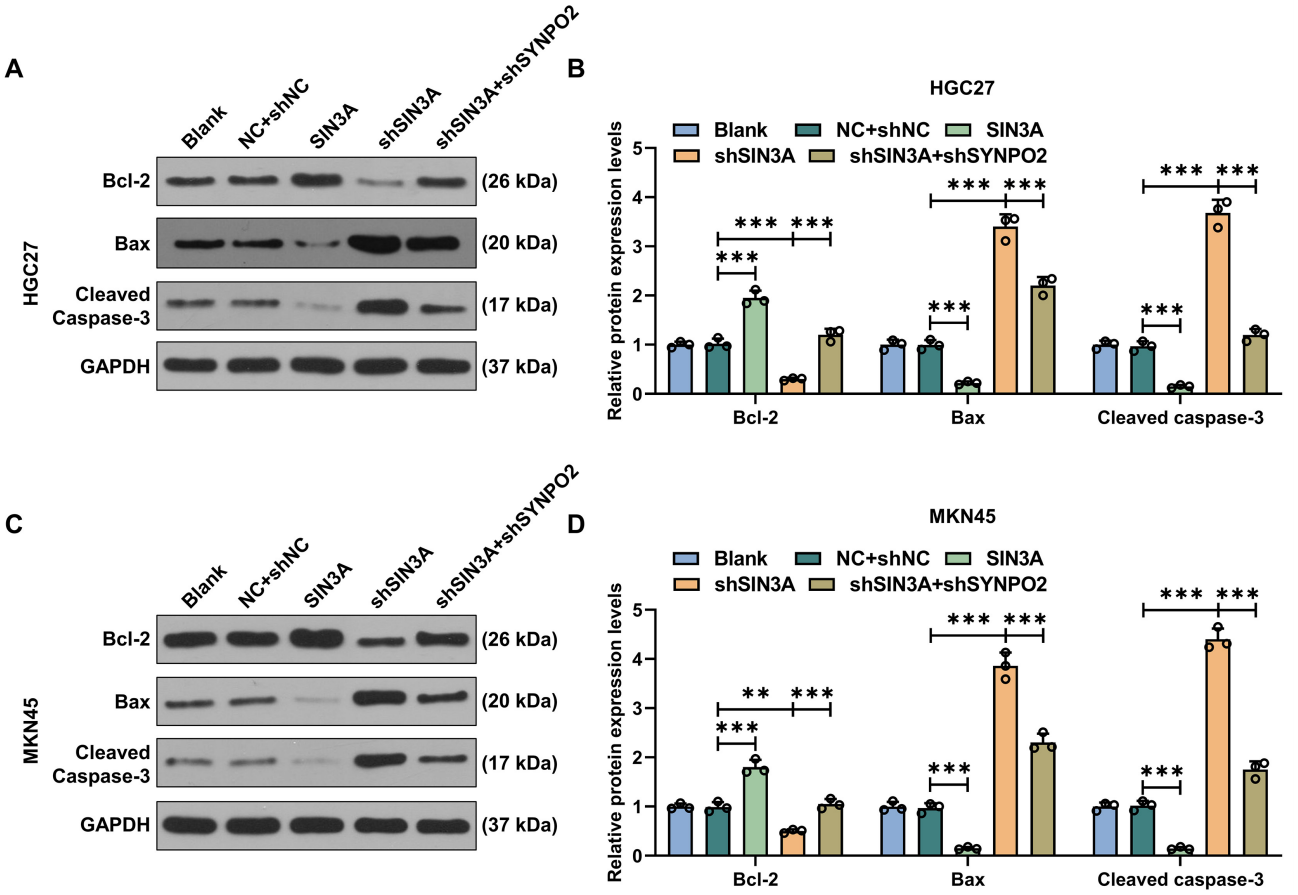

Fig. 8. *SIN3A*-mediated regulation of *SYNPO2* alters apoptosis-related protein expression in GC cells. (A,B) Protein expression levels of B-cell lymphoma 2 (Bcl-2), Bcl-2-associated X protein (Bax), and cleaved caspase-3 in HGC27 cells co-transfected with NC+shNC, shNC+*SIN3A* overexpression plasmids, NC+sh*SIN3A*, or sh*SIN3A*+sh*SYNPO2*, were analyzed by Western blotting (GAPDH as the loading control). (C,D) Detection of Bax, Bcl-2, and cleaved caspase-3 protein expression in MKN45 cells co-transfected with NC+shNC, shNC+*SIN3A* overexpression plasmids, NC+sh*SIN3A* or sh*SIN3A*+sh*SYNPO2* was analyzed by Western blotting (GAPDH as the loading control). $^{**}p < 0.01$, $^{***}p < 0.001$. n = 3.

of HDAC1 and HDAC2 to *SIN3A*, thereby transcriptionally repressing the expression of *SIN3A* target genes [24]. A previous study demonstrated that the *SIN3A*-HDAC repressor complex reduces the *HIF-2α* transcription in cancer cells via direct binding [36]. Thus, the *SIN3A*-HDAC repressor complex has been considered a potential therapeutic target in melanoma, with its pharmacological inhibition leading to suppression of metastatic tumor formation [37]. Furthermore, the *SIN3A*-HDAC repressor complex has also been implicated in the suppression of apoptosis in BC [38].

Consistently, our findings revealed that *SIN3A* functions as an oncogene in GC, positively correlating with cell proliferation, migration, and invasion, while negatively associated with GC cell apoptosis. Furthermore, we observed that *SYNPO2* knockdown reversed the inhibitory effects of *SIN3A* ablation on GC cell malignancy. Together with the known transcriptional regulatory role of *SIN3A*, this suggests that *SIN3A* silencing may relieve its transcriptional repression of *SYNPO2* to modulate GC cell malignant behavior. However, the precise mechanisms by which *SIN3A* regulates and inhibits *SYNPO2* transcription remain unknown. Notably, several studies have shown that *SYNPO2* promoter methylation suppresses its expression and is linked to poor prognosis in melanoma, bladder cancer, and colon cancer [13,39,40]. It has also been reported that *SIN3A* can influence DNA methylation through its interaction with enhancer of zeste homolog 2 (EZH2) [41]. *SYNPO2* intron sense-overlapping lncRNA (SYISL) has been found to impact myogenesis via an interplay with EZH2. Accordingly, *SIN3A* may regulate and inhibit *SYNPO2* transcription through methylation, a hypothesis that requires further experimental validation.

Conclusion

In conclusion, we demonstrate that knockdown of *SIN3A*, which is highly expressed in GC, suppresses GC progression *in vitro* by promoting the overexpression of *SYNPO2*, highlighting *SYNPO2* as a potential gene target for the development of novel therapies for GC patients. Fur-

ther investigations are warranted to assess *SIN3A* as a predictive biomarker for clinical outcomes. Moreover, future studies should investigate the relationship between *SIN3A* and *SYNPO2* mRNA and protein expression levels. Experimental validation using additional primary GC tissues, patient-derived samples, or *in vivo* models is also recommended in the future to substantiate our findings.

Availability of Data and Materials

The datasets generated during and analyzed during the current study are available from the corresponding author upon reasonable request.

Author Contributions

Substantial contributions to conception and design: FF, LQC. Data acquisition, data analysis and interpretation: QHX, JW, LRZ, WW. Drafting the article or critically revising it for important intellectual content: All authors. Final approval of the version to be published: All authors. Agreement to be accountable for all aspects of the work in ensuring that questions related to the accuracy or integrity of the work are appropriately investigated and resolved: All authors.

Ethics Approval and Consent to Participate

Not applicable.

Acknowledgment

Not applicable.

Funding

This work was supported by the 2023 Foshan Self-funded Science and Technology Innovation Project [2320001006803].

Conflict of Interest

The authors declare no conflict of interest.

Supplementary Material

Supplementary material associated with this article can be found, in the online version, at https://doi.org/10.24976/Discov.Med.202537198.108.

References

[1] Ni T, Chu Z, Tao L, Zhao Y, Zhu M, Luo Y, *et al*. PTBP1 drives c-Myc-dependent gastric cancer progression and stemness. British Journal of Cancer. 2023; 128: 1005–1018. https://doi.org/10.1038/s41416-022-02118-5.

[2] Yuan Z, Cui H, Wang S, Liang W, Cao B, Song L, *et al*. Combining neoadjuvant chemotherapy with PD-1/PD-L1 inhibitors for locally advanced, resectable gastric or gastroesophageal junction adenocarcinoma: A systematic review and meta-analysis. Frontiers in Oncology. 2023; 13: 1103320. https://doi.org/10.3389/fonc.2023.1103320.

[3] Liu CX, Gao Y, Xu XF, Jin X, Zhang Y, Xu Q, *et al*. Bile acids inhibit ferroptosis sensitivity through activating farnesoid X receptor in gastric cancer cells. World Journal of Gastroenterology. 2024; 30: 485–498. https://doi.org/10.3748/wjg.v30.i5.485.

[4] Ma YQ, Zhang M, Sun ZH, Tang HY, Wang Y, Liu JX, *et al*. Identification of anti-gastric cancer effects and molecular mechanisms of resveratrol: From network pharmacology and bioinformatics to experimental validation. World Journal of Gastrointestinal Oncology. 2024; 16: 493–513. https://doi.org/10.4251/wjgo.v16.i2.493.

[5] Bu ZJ, Wan SR, Steinmann P, Yin ZT, Tan JP, Li WX, *et al*. Effectiveness and Safety of Chinese Herbal Injections Combined with SOX Chemotherapy Regimens for Advanced Gastric Cancer: a Bayesian Network Meta-Analysis. Journal of Cancer. 2024; 15: 889–907. https://doi.org/10.7150/jca.91301.

[6] Norwood DA, Montalvan-Sanchez E, Dominguez RL, Morgan DR. Gastric Cancer: Emerging Trends in Prevention, Diagnosis, and Treatment. Gastroenterology Clinics of North America. 2022; 51: 501–518. https://doi.org/10.1016/j.gtc.2022.05.001.

[7] Sun QH, Kuang ZY, Zhu GH, Ni BY, Li J. Multifaceted role of microRNAs in gastric cancer stem cells: Mechanisms and potential biomarkers. World Journal of Gastrointestinal Oncology. 2024; 16: 300–313. https://doi.org/10.4251/wjgo.v16.i2.300.

[8] Zheng Z, Song Y. Synaptopodin-2: a potential tumor suppressor. Cancer Cell International. 2023; 23: 158. https://doi.org/10.1186/s12935-023-03013-6.

[9] Chalovich JM, Schroeter MM. Synaptopodin family of natively unfolded, actin binding proteins: physical properties and potential biological functions. Biophysical Reviews. 2010; 2: 181–189. https://doi.org/10.1007/s12551-010-0040-5.

[10] Beall B, Chalovich JM. Fesselin, a synaptopodin-like protein, stimulates actin nucleation and polymerization. Biochemistry. 2001; 40: 14252–14259. https://doi.org/10.1021/bi011806u.

[11] Kai F, Fawcett JP, Duncan R. Synaptopodin-2 induces assembly of peripheral actin bundles and immature focal adhesions to promote lamellipodia formation and prostate cancer cell migration. Oncotarget. 2015; 6: 11162–11174. https://doi.org/10.18632/oncotarget.3578.

[12] Jing L, Liu L, Yu YP, Dhir R, Acquafondada M, Landsittel D, *et al*. Expression of myopodin induces suppression of tumor growth and metastasis. The American Journal of Pathology. 2004; 164: 1799–1806. https://doi.org/10.1016/S0002-9440(10)63738-8.

[13] Gao L, van den Hurk K, Nsengimana J, Laye JP, van den Oord JJ, Beck S, *et al*. Prognostic Significance of Promoter Hypermethylation and Diminished Gene Expression of SYNPO2 in Melanoma. The Journal of Investigative Dermatology. 2015; 135: 2328–2331. https://doi.org/10.1038/jid.2015.163.

[14] OuYang C, Xie Y, Fu Q, Xu G. SYNPO2 suppresses hypoxia-induced proliferation and migration of colorectal cancer cells by regulating YAP-KLF5 axis. Tissue & Cell. 2021; 73: 101598. https://doi.org/10.1016/j.tice.2021.101598.

[15] Zhu Y, Wang X, Cui Y, Bai J, Zheng J, Fan Y. Vitamin C through upregulating SYNPO2 level suppresses the proliferation and migration of glioma cells. Journal of B.U.ON.: Official Journal of the Balkan Union of Oncology. 2021; 26. (online ahead of print)

[16] Chang SL, Yang CC, Lai HY, Tsai HH, Yeh CF, Lee SW, *et al*. SYNPO2 upregulation is an unfavorable prognostic factor for nasopharyngeal carcinoma patients. Medicine. 2023; 102: e34426. https://doi.org/10.1097/MD.0000000000034426.

[17] Gao J, Zhang HP, Sun YH, Guo WZ, Li J, Tang HW, *et al*. Synaptopodin-2 promotes hepatocellular carcinoma metastasis

via calcineurin-induced nuclear-cytoplasmic translocation. Cancer Letters. 2020; 482: 8–18. https://doi.org/10.1016/j.canlet.2020.04.005.

[18] Mazzocca M, Colombo E, Callegari A, Mazza D. Transcription factor binding kinetics and transcriptional bursting: What do we really know? Current Opinion in Structural Biology. 2021; 71: 239–248. https://doi.org/10.1016/j.sbi.2021.08.002.

[19] Saunders A, Huang X, Fidalgo M, Reimer MH, Jr, Faiola F, Ding J, *et al*. The SIN3A/HDAC Corepressor Complex Functionally Cooperates with NANOG to Promote Pluripotency. Cell Reports. 2017; 18: 1713–1726. https://doi.org/10.1016/j.celrep.2017.01.055.

[20] Hao Y, Song S, Li T, Zai Q, Ma N, Li Y, *et al*. Oxidative stress promotes liver fibrosis by modulating the microRNA-144 and SIN3A-p38 pathways in hepatic stellate cells. International Journal of Biological Sciences. 2024; 20: 2422–2439. https://doi.org/10.7150/ijbs.92749.

[21] Perucho L, Icardi L, Di Simone E, Basso V, Agresti A, Vilas Zornoza A, *et al*. The transcriptional regulator Sin3A balances IL-17A and Foxp3 expression in primary CD4 T cells. EMBO Reports. 2023; 24: e55326. https://doi.org/10.15252/embr.202255326.

[22] Mitra A, Vo L, Soukar I, Chaubal A, Greenberg ML, Pile LA. Isoforms of the transcriptional cofactor SIN3 differentially regulate genes necessary for energy metabolism and cell survival. Biochimica et Biophysica Acta. Molecular Cell Research. 2022; 1869: 119322. https://doi.org/10.1016/j.bbamcr.2022.119322.

[23] Bao L, Kumar A, Zhu M, Peng Y, Xing C, Wang JE, *et al*. SAP30 promotes breast tumor progression by bridging the transcriptional corepressor SIN3 complex and MLL1. The Journal of Clinical Investigation. 2023; 133: e168362. https://doi.org/10.1172/JCI168362.

[24] Kadamb R, Mittal S, Bansal N, Batra H, Saluja D. Sin3: insight into its transcription regulatory functions. European Journal of Cell Biology. 2013; 92: 237–246. https://doi.org/10.1016/j.ejcb.2013.09.001.

[25] Livak KJ, Schmittgen TD. Analysis of relative gene expression data using real-time quantitative PCR and the 2(-Delta Delta C(T)) Method. Methods (San Diego, Calif.). 2001; 25: 402–408. https://doi.org/10.1006/meth.2001.1262.

[26] Yan Y, Qian H, Cao Y, Zhu T. Nuclear factor-κB inhibitor Bay11-7082 inhibits gastric cancer cell proliferation by inhibiting Gli1 expression. Oncology Letters. 2021; 21: 301. https://doi.org/10.3892/ol.2021.12562.

[27] Machlowska J, Baj J, Sitarz M, Maciejewski R, Sitarz R. Gastric Cancer: Epidemiology, Risk Factors, Classification, Genomic Characteristics and Treatment Strategies. International Journal of Molecular Sciences. 2020; 21: 4012. https://doi.org/10.3390/ijms21114012.

[28] Sun BO, Fang Y, Li Z, Chen Z, Xiang J. Role of cellular cytoskeleton in epithelial-mesenchymal transition process during cancer progression. Biomedical Reports. 2015; 3: 603–610. https://doi.org/10.3892/br.2015.494.

[29] Linnemann A, Vakeel P, Bezerra E, Orfanos Z, Djinović-Carugo K, van der Ven PFM, *et al*. Myopodin is an F-actin bundling protein with multiple independent actin-binding regions. Journal of Muscle Research and Cell Motility. 2013; 34: 61–69. https://doi.org/10.1007/s10974-012-9334-5.

[30] Lu Y, Walji T, Ravaux B, Pandey P, Yang C, Li B, *et al*. Spatiotemporal coordination of actin regulators generates invasive protrusions in cell-cell fusion. Nature Cell Biology. 2024; 26: 1860–1877. https://doi.org/10.1038/s41556-024-01541-5.

[31] Kai F, Duncan R. Prostate cancer cell migration induced by myopodin isoforms is associated with formation of morphologically and biochemically distinct actin networks. FASEB Journal: Official Publication of the Federation of American Societies for Experimental Biology. 2013; 27: 5046–5058. https://doi.org/10.1096/fj.13-231571.

[32] Xia E, Zhou X, Bhandari A, Zhang X, Wang O. Synaptopodin-2 plays an important role in the metastasis of breast cancer via PI3K/Akt/mTOR pathway. Cancer Management and Research. 2018; 10: 1575–1583. https://doi.org/10.2147/CMAR.S162670.

[33] Pistritto G, Trisciuoglio D, Ceci C, Garufi A, D'Orazi G. Apoptosis as anticancer mechanism: function and dysfunction of its modulators and targeted therapeutic strategies. Aging. 2016; 8: 603–619. https://doi.org/10.18632/aging.100934.

[34] Sun Y, Chen Y, Zhuang W, Fang S, Chen Q, Lian M, *et al*. Gastric cancer peritoneal metastasis related signature predicts prognosis and sensitivity to immunotherapy in gastric cancer. Journal of Cellular and Molecular Medicine. 2023; 27: 3578–3590. https://doi.org/10.1111/jcmm.17922.

[35] Tang X, Yan T, Wang S, Liu Q, Yang Q, Zhang Y, *et al*. Treatment with β-sitosterol ameliorates the effects of cerebral ischemia/reperfusion injury by suppressing cholesterol overload, endoplasmic reticulum stress, and apoptosis. Neural Regeneration Research. 2024; 19: 642–649. https://doi.org/10.4103/1673-5374.380904.

[36] Biddlestone J, Batie M, Bandarra D, Munoz I, Rocha S. SIN-HCAF/FAM60A and SIN3A specifically repress HIF-2α expression. The Biochemical Journal. 2018; 475: 2073–2090. https://doi.org/10.1042/BCJ20170945.

[37] Min D, Byun J, Lee EJ, Khan AA, Liu C, Loudig O, *et al*. Epigenetic Silencing of BMP6 by the SIN3A-HDAC1/2 Repressor Complex Drives Melanoma Metastasis via FAM83G/PAWS1. Molecular Cancer Research: MCR. 2022; 20: 217–230. https://doi.org/10.1158/1541-7786.MCR-21-0289.

[38] Yang Y, Huang W, Qiu R, Liu R, Zeng Y, Gao J, *et al*. LSD1 coordinates with the SIN3A/HDAC complex and maintains sensitivity to chemotherapy in breast cancer. Journal of Molecular Cell Biology. 2018; 10: 285–301. https://doi.org/10.1093/jmcb/mjy021.

[39] Alvarez-Múgica M, Cebrian V, Fernández-Gómez JM, Fresno F, Escaf S, Sánchez-Carbayo M. Myopodin methylation is associated with clinical outcome in patients with T1G3 bladder cancer. The Journal of Urology. 2010; 184: 1507–1513. https://doi.org/10.1016/j.juro.2010.05.085.

[40] Esteban S, Moya P, Fernandez-Suarez A, Vidaurreta M, González-Peramato P, Sánchez-Carbayo M. Diagnostic and prognostic utility of methylation and protein expression patterns of myopodin in colon cancer. Tumour Biology: the Journal of the International Society for Oncodevelopmental Biology and Medicine. 2012; 33: 337–346. https://doi.org/10.1007/s13277-012-0320-8.

[41] Bisserier M, Mathiyalagan P, Zhang S, Elmastour F, Dorfmüller P, Humbert M, *et al*. Regulation of the Methylation and Expression Levels of the BMPR2 Gene by SIN3a as a Novel Therapeutic Mechanism in Pulmonary Arterial Hypertension. Circulation. 2021; 144: 52–73. https://doi.org/10.1161/CIRCULATIONAHA.120.047978.